Traffic

Published by John Wiley & Sons Ltd
doi:10.1111/tra.12307

Microtubule C-Terminal Tails Can Change Characteristics of Motor Force Production

Mitra Shojania Feizabadi[1,2], Babu Reddy Janakaloti Narayanareddy[2], Omid Vadpey[2], Yonggun Jun[2], Dail Chapman[2], Steven Rosenfeld[3] and Steven P. Gross[2]

[1] *Department of Physics*, *Seton Hall University*, South Orange, NJ 07079, USA
[2] *Department of Developmental and Cell Biology*, *University of California*, Irvine, CA 92697, USA
[3] *Department of Cancer Biology*, *Cleveland Clinic*, Cleveland, OH, USA
*Corresponding authors: *Mitra Shojania Feizabadi,* shojanmi@shu.edu *and Steven P. Gross,* sgross@uci.edu

Abstract

Control of intracellular transport is poorly understood, and functional ramifications of tubulin isoform differences between cell types are mostly unexplored. Motors' force production and detachment kinetics are critical for their group function, but how microtubule (MT) details affect these properties – if at all – is unknown. We investigated these questions using both a vesicular transport human kinesin, kinesin-1, and also a mitotic kinesin likely optimized for group function, kinesin-5, moving along either bovine brain or MCF7(breast cancer) MTs. We found that kinesin-1 functioned similarly on the two sets of MTs – in particular, its mean force production was approximately the same, though due to its previously reported decreased processivity, the mean duration of kinesin-1 force production was slightly decreased on MCF7 MTs. In contrast, kinesin-5's function changed dramatically on MCF7 MTs: its average detachment force was reduced and its force–velocity curve was different. In spite of the reduced detachment force, the force–velocity alteration surprisingly improved high-load group function for kinesin-5 on the cancer-cell MTs, potentially contributing to functions such as spindle-mediated chromosome separation. Significant differences were previously reported for C-terminal tubulin tails in MCF7 versus bovine brain tubulin. Consistent with this difference being functionally important, elimination of the tails made transport along the two sets of MTs similar.

Keywords C-terminal, Eg5, force production, kinesin-1, microtubule

Received 5 March 2015, revised and accepted for publication 16 June 2015, uncorrected manuscript published online 22 June 2015

The kinesin family of proteins has diverse cellular functions. Motors such as kinesin-1 ('Kin-1') play critical roles in cargo transport and organelle positioning, and in cells they typically function predominantly in the small *n* (~1–6) limit (1–4). In contrast, kinesins such as kinesin-5 (Eg5, henceforth 'Kin-5') play critical roles in mitosis, with high-force applications requiring teams of many (>100) motors (5,6).

While kinesin-family motor domains are relatively conserved, there are still significant differences in the motors kinetic cycles and also their necks and neck-linkers (7–14), and we are only starting to understand the extent to which molecular variations adapt the motors to their specific functions (see e.g. 15–18). Such adaptations may change how the motors interact with different classes of microtubules (MTs), and while some reports have found little effect on single-molecule properties of Kin-1 (19,20), there is evidence that post-translational modifications can alter transport (see e.g. 21–25).

Most studies to date using purified components (*in vitro*) have been carried out using neuronal sources of tubulin, so how motor function depends on isoform/cell specific variation in tubulin remains unknown. Importantly, a recent study using recombinant tubulin isoforms (26) established that single-motor processivities can be affected, consistent with the general hypothesis that cell-specific variation may indeed matter. Whether such isoform variation affects

characteristics of force production, and if so how and why, remains unexplored.

In most cases, motors do not function in isolation, but instead function in groups (27–31). Our recent studies (32,33) highlighted the importance of single-motor detachment under load, as well as the contribution of lower velocities, to increased group function (34). Thus, we wondered whether motors that function in large groups (e.g. Kin-5) might respond differently than motors that function in small numbers (Kin-1) when encountering different MT substrates. To address this, we studied Kin-1 and Kin-5 under well-controlled conditions *in vitro*, moving along bovine versus MCF7 MTs, and in particular examined how the presence of load (opposition to motion) affected each class of motor.

Results

We first studied single Kin-1 (KIF5B) 1–560 aa motors (henceforth 'K560') attached to beads, moving along either bovine or MCF7 MTs. We previously reported that under no load, K560's processivity on MCF7 MTs was reduced by approximately 50% while its velocity remained unchanged (35). We now studied the effect of load, by keeping the optical trap engaged. As the motor pulled the bead toward the edge of the trap, the load increased, until the motor either stalled or detached. As expected, as the load increased, the mean velocity decreased. We did not carefully quantify the force–velocity curve, but detected no large differences in behavior along bovine versus MCF7 MTs. The previously reported decrease in processivity along MCF7 under no load was confirmed, and somewhat increased the probability of detachment under load as well. Thus, along MCF7 MTs the motors were slightly more likely to detach before stalling, so the typical detachment force of K560 along MCF7 was slightly reduced relative to K560 functioning along bovine MTs. We did not extensively quantify the exact stalling force in each case but it is likely not significantly changed, as typical maximal forces observed in each case were similar (Figure S1, examples in (A) and (B), and histogram of peak forces in (C) and (D)).

The total duration of attachment of single-motors under load contributes to group function (32–34): the longer a motor remains bound, the higher the probability of other detached motors rebinding before the bound motor detaches. Thus, we quantified the single-motor total binding time. Consistent with decreased processivity, durations of K560 events on MCF7 MTs were somewhat reduced relative to the same events on bovine MTs (Figure S1E,F). Thus, along MCF7 MTs, cargos moved by multiple single kinesin-1 motors would be expected to have slightly reduced travel and force production due to the expected slight decrease in instantaneously engaged motors.

We next studied motion of a dimeric Eg5-Kinesin 1 chimera with Eg5 motor domain, neck, and neck linker, henceforth referred to as 'Eg5'. We and others (36–38) have used this type of chimeric construct to reliably measure processivity at the single molecule level. Unlike the modest (at most) effect of MCF7 on kin-1 force production, for Eg5 the effect was quite substantial: on MCF7 MTs Eg5 motors were clearly more prone to detach (Figure 1A,B) leading to a dramatic decrease in mean detachment force (Figure 1C,D). To our surprise, even though the motors detached at a lower peak force, the mean duration of attachment events was essentially the same for single-motor travel along bovine versus MCF7 MTs (Figure 1E,F).

The maintenance of long event duration on MCF7 MTs is of obvious utility for multiple-motor function (allowing increased probability of rebinding of detached motors, to increase mean number of engaged motors; see also modeling, below), so we wondered how it was achieved, given the motors' shorter travel distance. One possibility was that the overall velocity was slower, so we looked at unloaded velocities of Eg5 on bovine versus MCF7 MTs, and discovered they were the same, and approximately 90 nm/seconds (Figure 2E).

Since unloaded velocity was the same, we next hypothesized that perhaps Eg5's force-velocity curve was altered on MCF7 MTs. The velocity of Eg5 moving along bovine MTs is reported to be relatively insensitive to load (5), a finding we confirmed (Figure 2A,B, and compare red curves in Figure 2E–G). Upon quantification, we discovered this was not true for Eg5 along MCF7 MTs: there was significant slowing down in response to load, both in individual traces (Figure 2C,D) and in the overall distributions of high-load versus low-load velocities (compare black histograms/curves in Figure 2E–G). Thus, in response to load,

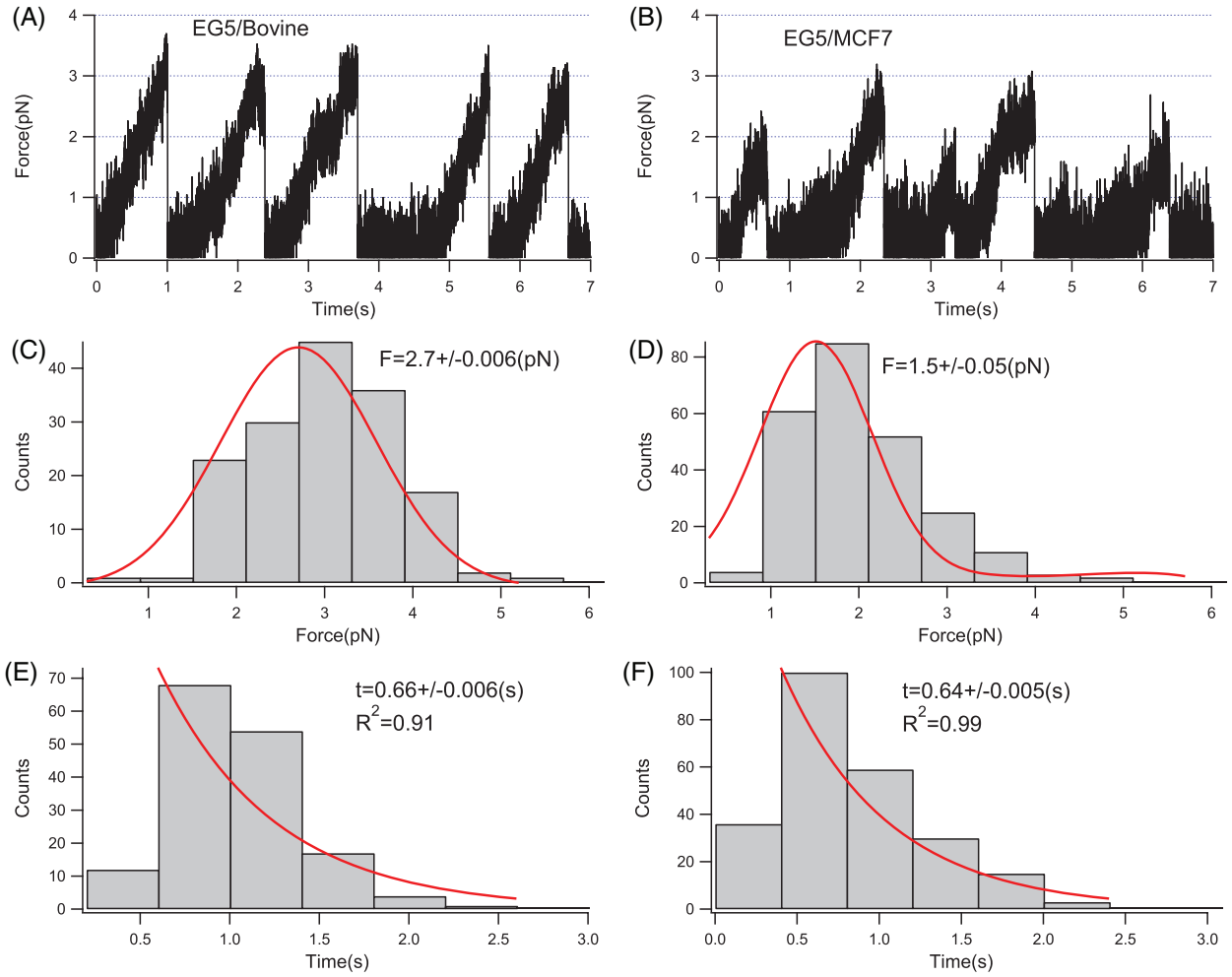

Figure 1: Characterization of Eg-5 moving along bovine brain and MCF7 microtubules. Example force versus time traces of Eg5-coated beads moving along a single (A) bovine brain microtubule or (B) MCF7 microtubule, under a moderately high-force optical trap (trap stiffness of ∼0.05 pN/nm). Experiments were performed at saturating (1 mM) ATP. Histogram of forces produced along (C) bovine brain and (D) MCF7 microtubules are shown. The average detachment force is calculated by fitting the Gaussian distribution to the histograms, found to be is 2.7 ± 0.006 pN on bovine brain microtubules ($n = 156$ measurements, C) and 1.5 ± 0.05 pN ($n = 243$ measurements, D) on MCF7 microtubules. The mean value of forces in (C) and (D) are extremely significantly different, as determined by *t*-test. The distribution of binding times along the two types of microtubules is shown in (E) and (F), and in each case was well described by a decaying exponential (red), with value of 0.66 ± 0.006 seconds (bovine) and 0.64 ± 0.005 seconds (MCF7).

when moving on MCF7 MTs, Eg5 motors slow down dramatically, allowing them to spend approximately the same time bound to the MT, in spite of going a shorter distance before detaching.

In principle, the increased ability to sustain high load without detaching can lead to strain-gating (39), allowing better force-sharing among motors, with the overall effect of enhancing multiple-motor co-operation and ensemble force production. To test this possibility, we incubated beads with different amounts of Eg5 motors, and tested them in parallel on bovine and MCF7 MTs. At a dilution of 1:10 000 we had a bead binding fraction of ∼0.4, and were in the single-molecule regime (labeled 1× in Figure 3). In this case, as in Figure 1, we again found that single Eg5 motors produced a higher peak force on bovine MTs, but that the duration of events was approximately the same on both sets of MTs. We then went to a dilution of 1:1000 (10×

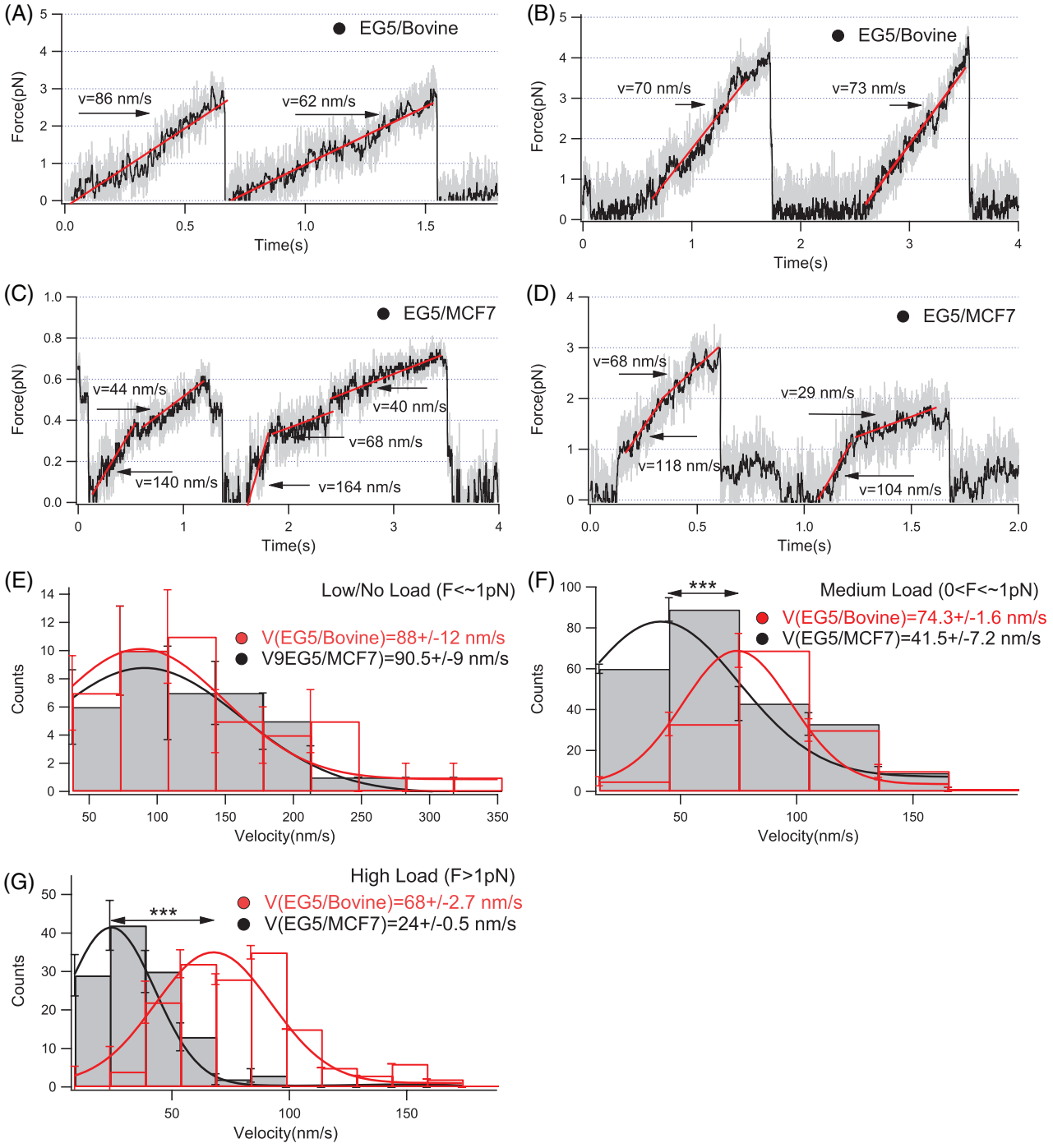

Figure 2: Quantization of Eg-5-coated beads moving in an optical trap along bovine and MCF7 microtubules. In the example traces, it appears that velocity is approximately independent of load along bovine MTs (A, B), but decreases with load along MCF7 MTs (C, D). This general trend was confirmed by quantifying velocity for many such traces, for low-load (E, Force < 0.5 pN, $n = 45$ [bovine] and $n = 37$ [MCF7]), moderate load (F, ~0.5 < Force < 1 pN, F, $n = 156$ [bovine] and $n = 243$ [MCF7]), and higher load (G, Force > 1 pN, $n = 152$ [bovine] and $n = 119$ [MCF7]). *** Significantly different mean values, as determined by *t*-test.

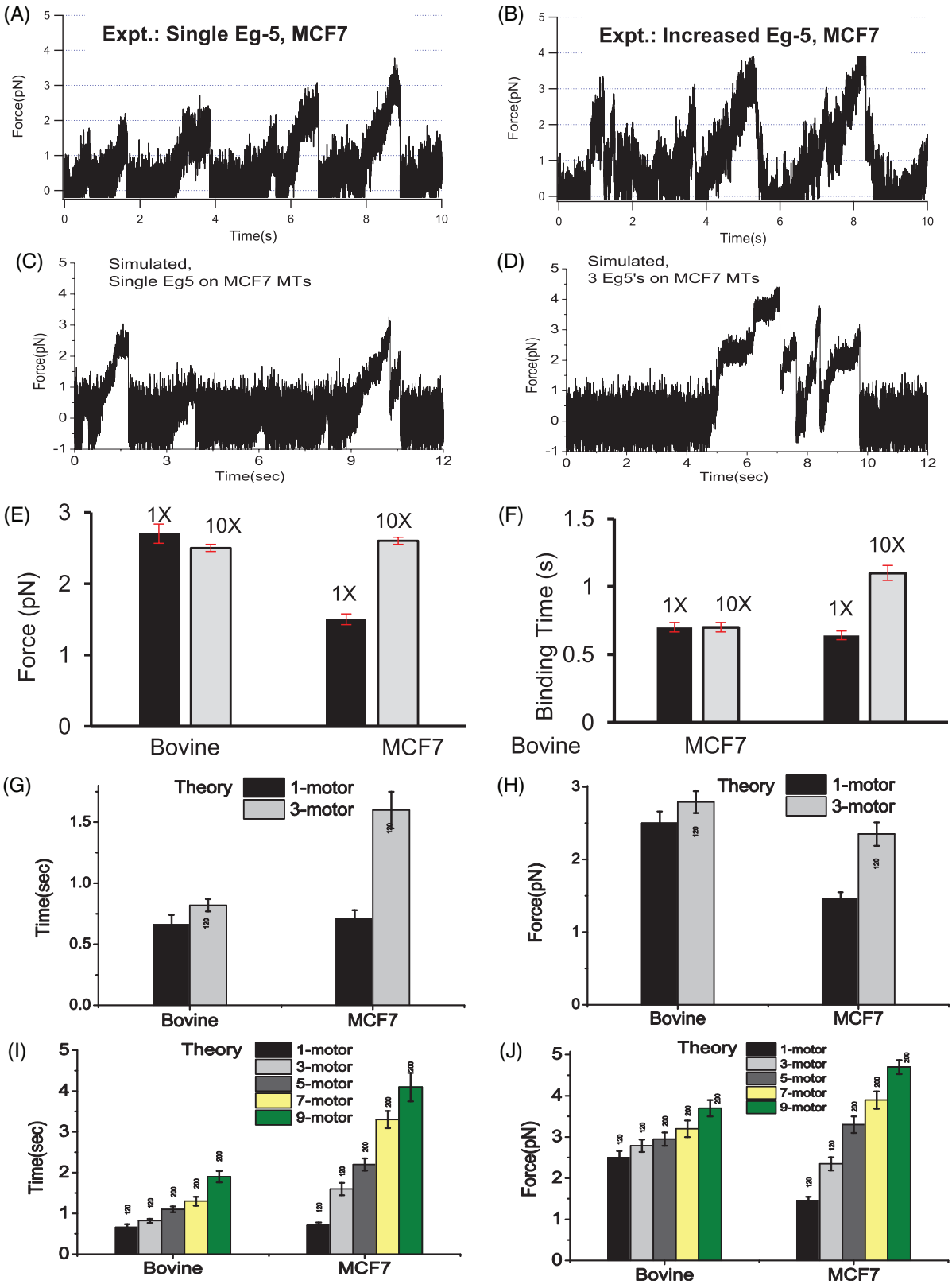

Figure 3: Legend on the next page.

in Figure 3). As expected, the binding fraction increased to 1. We do not know the exact number of motors per bead, but a number of observations confirmed that we were now in the multiple-motor range. First, self-recruitment of beads to MTs was observed (in contrast to the necessity to place beads on MTs with the optical trap, as required in single-molecule experiments). Second, travel distances of beads moving under no load increased (not shown). Third, the time between attempts for a bead held close to the MT decreased (Figure S5, compare left versus right top panels). Finally there were occasional force attempts larger than the 3 pN we see for single Eg5 motors (Figure S5, compare top left and right panels). Then, in parallel assays, we quantified average force production of identical beads along both types of MTs. The presence of additional motors improved force production dramatically on MCF7 MTs but not on the bovine MTs: for MCF7 MTs, average maximal force production doubled, but was approximately unchanged for bovine MTs (Figure 3 A,B,E). Furthermore, in contrast to the single-molecule case where force production duration was the same on each set of MTs, for the multiple-motor case force production lasted considerably longer on MCF7 MTs (Figure 3F). Thus, on bovine MTs, although we do see hints of the second motor's activity in individual traces (Figure S5), *on average* the additional motors' contribution is not large as far as force production. In contrast, the additional motors play a more significant role on MCF7 MTs. We attribute these differences to the effect of distinct force–velocity curves in helping motors co-ordinate their activity (see *Modeling*, *Role of the C-terminal tails* and *Discussion* sections).

Modeling

When Eg5 motors function in cells to set up spindles, they work in large groups, but experimentally in multiple-motor bead experiments, with randomly attached motors, we can only reach moderate numbers (likely $n \sim 3$) of simultaneously engaged motors. Thus, we first validated a theoretical modeling/simulation approach by determining that the observed changes in the single-motor force–velocity curve were enough to theoretically account for the experimentally observed differences, and then used the same theory to extrapolate function for larger n values. We started by simulating a single Eg5 moving along either a bovine or MCF7 MT. The critical difference was the shape of the force–velocity curve, with the modeled 'bovine' Eg5 having a velocity insensitive to load, and the 'MCF7' Eg5 being much more sensitive to load. The simulation parameters were tuned so that the simulations of single Eg5 motors moving a bead in an optical trap matched the experimental data (mean maximum force and mean duration of the event) shown in Figure 1A, B. Once the parameters for the single-motor models were determined, we now put multiple simulated motors together as we did previously (39).

Based on past multiple-motor bead experiments with kinesin (40), we expected that in the multiple-motor limit we are likely to have approximately three motors engaged. Thus, using the same on-rate as was used for modeling multiple kinesins (34), we simulated three Eg5 motors moving on either bovine or MCF7 MTs, and found that theory matched the experiment quite well (Figure 3A–H). That is, the average force production and duration of force attempts did not increase very much for Eg5 moving on bovine MTs, but did increase for Eg5 on MCF7 MTs. As the only difference between the two sets of simulations was the shape of the force–velocity curve, and the magnitude of the increase for the MCF7 was consistent with what was observed experimentally, these simulations suggest that indeed the difference in the force–velocity curve is enough to account for the experimentally observed differences in bead force production at higher Eg5 concentrations.

Figure 3: Theory and experiment for multiple Eg5 motors on bovine and MCF7 MTs. (A, B) Experimental traces of Eg5 motors in an optical trap, moving on MCF7 microtubules (A) at single molecule level and (B) at higher concentration. Example simulation trace of (C) single and (D) multiple Eg5 motors tracks on MCF7 microtubules in an optical trap (0.05 pN/nm). Quantization of changes in experimental mean detachment (E) forces and (F) times for single and multiple Eg5 motors on bovine and MCF7 microtubules. Quantization of simulated motion (G, H) agrees with experiments. Simulations were then used to extrapolate mean force production (I) and mean duration of force production for larger numbers of Eg5 motors on bovine and MCF7 microtubules. Number above bars (I, J) reflect total binding events simulated, with all $n \geq 120$. A typical event includes the motor binding to the microtubule, walking away from trap center and detaching.

With the simulations thus experimentally validated, we now went to even higher n-values ($n = 5, 7, 9$) (Figure 3I,J). We found that simulations support the general model that the mean magnitude of force production and mean duration of force attempts both increase more significantly for the MCF7-Eg5 than for the bovine-Eg5, suggesting that the Eg5-MCF7 force–velocity curve does indeed promote improved multiple-motor function. Thus, our single-molecule data combined with simulations suggest that by altering force–velocity relations, different MT isoforms may contribute to overall cellular force production in surprising ways, and in particular details of the MTs can alter the way motors combine their forces.

Role of post-translational modifications

Mechanistically, what is likely to account for the differences of Eg5 function along MCF7 versus bovine brain MTs? As tubulin can undergo post-translational modifications, one possibility is that the MCF7 tubulin is modified differently than the bovine brain MTs. To assess this, we used a suite of modification-specific antibodies. Grossly, we observed no obvious difference in the amount of each modification (Figure S2); more quantitatively, using these western blots, we measured the intensity of each band, and normalized it by the intensity of the overall tubulin band (Figure 4A). In each case, the magnitude of the specific post-translational modification signal is roughly the same, when comparing MCF7 to bovine MTs. Thus, we believe that differences in post-translational modifications are unlikely to explain the majority of the observed functional differences. Nonetheless, some contribution (especially from tyrosination which appears the most different) cannot be ruled out. Although there is a weak band in the MCF7 gel (Figure 4C) at ~116 kDa, it is at quite low concentration relative to the normal tubulin band at ~50 kDa, and we believe it is likely tubulin dimers that failed to separate, because it is recognized by the antitubulin antibody. It is thus unlikely to account for the differences, especially in light of the effects of subtilisin treatment (see *Role of the C-terminal tails* section).

Role of the C-terminal tails

There is known to be significant diversity of β-tubulin isoforms, differing predominantly in the carboxy-terminal tail region (26,41,42). Thus, we wanted to determine whether these differences might explain the differences

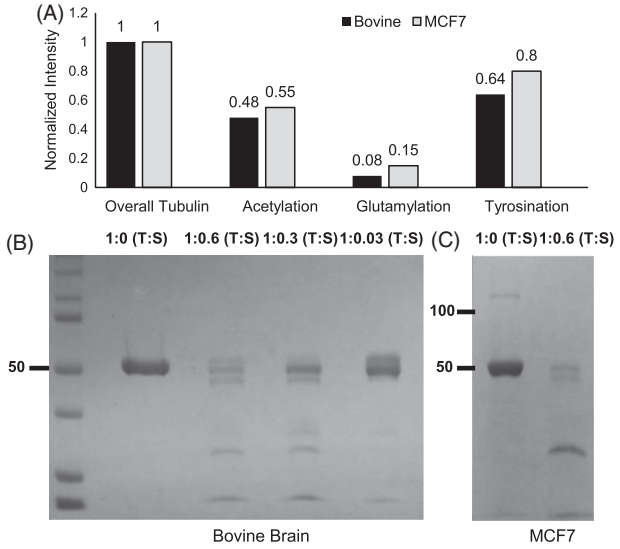

Figure 4: Post-translational modifications and subtilisin treatment analysis. (A) Western blots of both bovine and MCF7 tubulin modifications (Figure S2) were quantified using ImageJ software. The values were normalized to the overall tubulin intensity. The results of this analysis, shown in (A), indicate that levels of post-translational modifications are similar on bovine versus MCF7 tubulin. (B) Microtubules polymerized from bovine tubulin were treated with different ratios of subtilisin (w/w). Most effective for our studies was a ratio of Tubulin(T):Subtilisin(S) of 1:0.6 (w/w), which was subsequently used for the treatment of MCF7 microtubules as shown in (C). ImageJ analysis indicates that the ~116 kDa band (panel C – left) is less than 10% of total MCF7 tubulin.

in Eg5 function on the two types of MTs. To test this, we followed previous work (43), using subtilisin digestion (Figure 4B,C) to remove the tubulin tails. We then measured single-molecule Eg5 function on subtilisin-treated bovine ('S-bovine') and MCF7-MTs ('S-MCF7').

Strikingly, subtilisin treatment changed the apparent force–velocity curve of Eg5 on bovine MTs: although velocity is insensitive to load on untreated bovine MTs (Figure 2), it has become more sensitive to load on S-bovine MTs (Figures 5A and S3A), similar to motion on untreated MCF7 MTs (Figure 2). Furthermore, load sensitivity of Eg5 on subtilisin-treated MCF7 MTs was essentially unchanged (Figures 5B and S3B) suggesting that MCF7 tubulin tails lack what is required to promote load insensitivity.

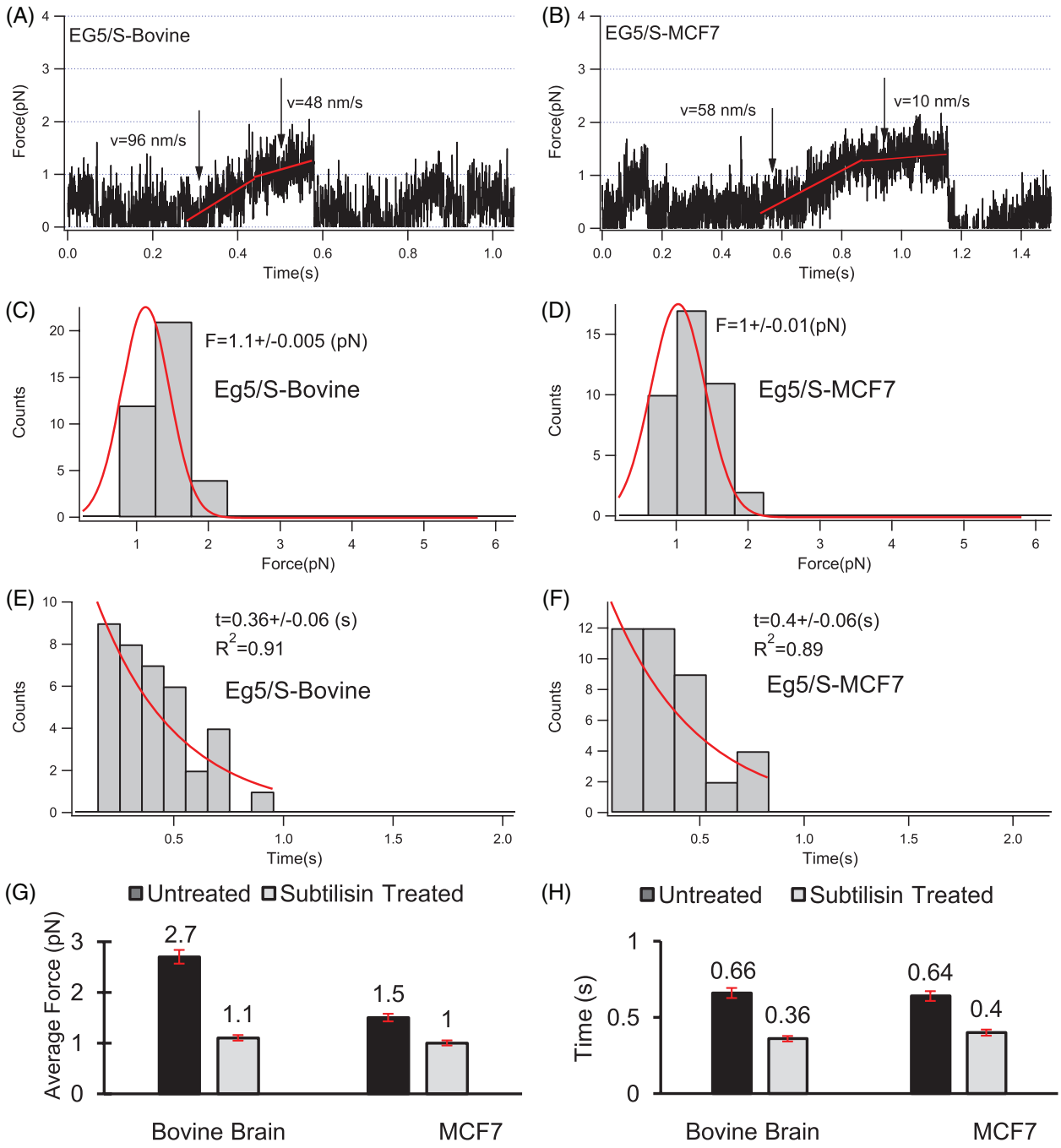

Figure 5: Characterization of EG5 moving on subtilisin-treated bovine brain and MCF7 microtubules. Example force versus time traces of single EG5 motors moving beads at saturating (1 mM) ATP along subtilisin-treated bovine brain (A) (see also Figure S3A) or MCF7 (B) MTs in an optical trap (trap stiffness ~0.05 pN/nm). Histograms of forces produced along these treated brain (C) and (D) MCF7 microtubules are shown. The average detachment force on S-bovine brain (1.1 ± 0.005 pN, $n = 37$, C) and on S-MCF7 microtubules (1 ± 0.01 pN, $n = 40$, D) was calculated by fitting the Gaussian distribution to the histograms. The binding time distributions are shown in (E) and (F), and in each case was well described by a decaying exponential (red), with value of 0.36 ± 0.06 seconds (bovine) and 0.4 ± 0.06 seconds (MCF7). (G, H) Average detachment forces and binding times for single EG5 motors on different substrates (summarizing data from Figures 1 and 5) are compared.

Thus, we hypothesized that the presence of the bovine tails is required to maintain the insensitivity of velocity to load. If indeed the presence of the bovine C-terminal tails accounts for much of the difference between function on bovine and MCF7 MTs, one might then expect that upon removal of the tails, (i) function of Eg5 on S-bovine might be similar to motion on S-MCF7 and (ii) subtilisin treatment ought to have more of an effect on Eg5 function for bovine as compared to MCF7 MTs. We tested both these predictions by quantifying average maximal force production in each case (Figure 5C,D). Indeed, mean force production was more reduced for Eg5 on S-bovine (1.1 pN-Figure 5C) relative to bovine (2.7 pN-Figure 1C), as compared to the minimal effect on force production for Eg5 on S-MCF7 (1pN-Figure 5D) versus MCF7 (1.5 pN-Figure 1D); summary in Figure 5G. Furthermore, the maximal force production was now approximately the same for Eg5 on S-bovine and S-MCF7 (∼1 pN); Figure 5G. Subtilisin treatment also decreased Kin-1 force production on both classes of MTs (Figure S4). Finally, for both classes of motors on both types of MTs, subtilisin treatment slightly decreased the duration of force producing events (Figures 5 E,F and S4E,F versus Figure S1E,F), summarized in Figure 5H, implicating the tails in contributing to control of the duration of force production as well as its magnitude.

Discussion

In cells, there is known to be significant diversity of β-tubulin isoforms, differing predominantly in the carboxy-terminal tail region (26,41,42). Tubulin's carboxy-terminal tails are interesting because although they are not the primary binding site for motors, their loss (via subtilisin digestion) is established to alter unloaded travel distances of multiple-motor beads (43), and also single-motor velocity and processivity (26).

Thus, there is significant evidence supporting a relationship between motor processivity and tubulin isoform. However, until now the functional ramifications of different tubulin isoforms with regard to motor force production in both the single-molecule and multiple-motor regimes remained unexplored. Here, we were particularly interested in isoforms reflecting cancerous versus neuronal MTs: bovine brain MTs have predominantly the βII isoform (58%) with almost no βI and βIV tubulin (∼3 and ∼13%, respectively) (41) whereas cancerous cells predominantly have βI and βIV tubulin (∼90 and 10% for HeLa cells, and ∼55 and 39% for MCF-7 cells) (34).Thus, we investigated how the function of a vesicular transport kinesin (Kin-1) and a mitotic kinesin (Kin-5) changed, when moving along bovine versus MCF7 MTs.

We found that while MCF7 MTs decreased travel for both kin-1 and Kin-5, Kin-5 appeared to compensate for the shorter travel by slowing down under load, allowing it to remain attached for the same duration on both classes of MTs. Surprisingly, by allowing it to spend more time on average bound to the MT when under high load (as compared to Kin-5 on bovine MTs), this alteration actually *improved* high-load system-level performance for multiple Kin-5s on MCF7 MTs (Figure 3), allowing improved additivity of force production.

A number of findings seemed noteworthy from this study. The first is the discovery that a motors' force-velocity curve may be strongly dependent on the nature of the MT track, and indeed, on the C-terminal tails as suggested by our subtilisin data. Effects on processivity were not unexpected based on other work (26), but the sensitivity of the shape of the force-velocity was surprising. Certainly, this will be interesting to explore in the future.

Second, the observation that although the motors are relatively conserved structurally, they could be differentially affected (Kin-1's force–velocity behavior was approximately the same on the two classes of MTs) was intriguing. Some of the kinetic differences in the enzymatic cycles of Kin-1 versus Eg5 highlighted in a recent study (11) may ultimately help understand this difference.

Third, the study is consistent with the hypothesis that the tubulin tails may play an important role in determining Kin-5's force–velocity curve, both because the subtilisin data implicates either the alpha or beta-tails in contributing to the Kin-5 force–velocity curve, and because the C-terminal tails of the beta-tubulin are reported to be quite different between bovine and MCF7 tubulin (see above). Nonetheless, as we have not directly tested the beta-tubulin tails, other possibilities cannot be disregarded.

Finally, there has been interest in understanding how well multiple motors function together. Some work suggests kinesin motors do not combine forces well (44) while other studies suggest forces are additive (28). Our findings here – both experimental and theoretical – highlight the importance of the single-motor force–velocity curve on ensemble function consistent with proposals from a number of groups (32,39,44–46). Specifically, by changing the substrate they moved on, we were able to change Kin-5's single-motor force–velocity curve, and for identical numbers of motors, this dramatically changed the way they functioned together – on bovine MTs Kin-5 motors did not slow down significantly, so under load they detach rapidly, and forces do not add well (Figure 3). In contrast, on MCF7 MTs the same Kin-5 motors slow down under load and thus spend more time at higher load, allowing them to better combine forces, resulting in good addition of forces and concomitant larger increases in mean binding times with increasing numbers of motors (Figure 3).

Materials and Methods

Eg5 construct

The Eg5 motor used in these studies is a dimeric construct, composed of the Eg5 motor domain, neck linker and neck coiled coil fused to the hinge and coiled coil tail of kinesin 1. In particular, this construct fuses residues 1–402 from human Eg5 to residues 372–560 of kinesin 1. This insert encoding for this chimera was chemically synthesized and inserted into a pET21A expression vector (GenScript). The encoded protein was expressed in transformed *Escherichia coli* and purified by affinity chromatography using NiAgarose, as described in Ref 11.

Human Kin-1 construct

Expression construct of Kin-1 was Kif5b aa 1–560, pET17b-KIN-1-6xhis, was constructed using plasmid pET17b_Kin-1_GFP_his (Addgene) as template. Nde1 and Xho1 sites were used as restriction sites and the DNA oligo sequences used for PCR are listed as 5′-GATATACAT ATGGCGGACCTGGCCGAG, and 5′-GCGGGGCTCGAGTTAATGGT GGTGGTGATGAT GTTTTAGTAAAGATGCCATCATC. Vector pET17 was obtained from Novagen. Bacteria strain XL1-blue competent cells (Stratagene) was used for the transformation of pET17b-Kin-1-6xhis. Sequence-verified constructs was transformed into *E. coli* strain BL21 DE3 Rosetta for protein expression. Cells were selected by ampicilin and chloramphenicol, induced for expression at 18°C, lysed by sonication in ice water, and clarified by ultra centrifugation at 30 000 RCF. Protein was purified by Ni-NTA affinity column by first washing with 50 mM phosphate buffer pH 8.0, 300 mM NaCl and 75 mM Imidazole, and eluted out with 50 mM phosphate buffer pH 8.0, 300 mM NaCl and 250 mM Imidazole (34).

Experiment

The general procedure, which has previously been explained for kinesin (35), was modified to include also a second molecular motor, Eg5. Here, although most studies were carried out with a moderately high-force setting higher laser power (~110 mW, with corresponding trap stiffness of ~0.05 pN/nm), a few experiments were also performed in a lower force regime (laser power [~20 mW], with corresponding trap stiffness of ~0.005 pN/nm).

Details of reagents and approaches were as summarized in the following sections.

MT*s*

Bovine brain tubulin (Cytoskeleton, Cat. TL238A) and human breast cancer tubilin (cytoskeleton, Denver, Cat. H005) were polymerized, Taxol stabilized, diluted and immobilized on the channel of the polylysine-coated coverslip of fellow chambers. Kinesin-1 and Eg5 solutions were thawed and diluted with the assay buffer (66.4 mM pipes, pH 6.9/50 mM potassium acetate/3.4 mM $MgSO_4$/0.8 mM DTT/0.84 mM EGTA/10.1 μM Taxol). We implemented a series of dilutions for each motor to achieve ~single-motor/bead, with a bead binding fraction of approximately 33%. The necessary dilution ratio was identified for kinesin-1 and kinesin-5 separately. On the day of experimentation, polystyrene beads (489-nm diameter; Polysciences) were incubated with appropriately diluted kinesin-1 or kinesin-5 in the presence of 10 μM MgATP for almost 20 min. An oxygen scavenging solution (250 μg/mL glucose oxidase, 30 μg/mL catalase and 4.6 mg/mL glucose) was added to the solution of motor-polystyrene coated beads just before they were added to the bovine brain or MCF7 MTs (40,47,48).

The MTs and beads were visualized with differential interference contrast optics and were imaged at 30 fps with a CCD camera. The beads were trapped in an optical trap, which was then used to bring the bead in contract with an individual MT. Those beads with an active kinesin then bound to the MT and created movement of the trapped beads. These movements were recorded with a custom LabView program (49). The data were collected and analyzed by Igor-Pro software.

Subtilisin treatment

Both bovine brain and MCF7 MTs were incubated with subtilisin at the ratio 1:0.6 (w/w of tubulin:subtilisin) in accordance with the previously reported procedure (43).

SDS–PAGE gel

The purity of bovine brain tubulin and MCF7 tubulin as well as the enzymatic reaction of subtilisin on polymerized MTs were assessed by running the SDS gel.

Post-translational modifications of tubulin western blot

To understand the relative percentage of post-translational modifications of Bovine and MCF7 tubulin, tubulin samples were resolved on a two

10% SDS–PAGE followed by transfer onto 0.45 nitrocellulose membranes (Amersham). Membranes were blocked for 1 h at room temperature in 5% non-fat milk in TBS. Blots were then divided into strips and incubated for 2 h with the respective tubulin modification monoclonal primary antibodies (1:1000) at 4°C followed by goat anti-mouse secondary fluorescent-conjugated antibody (1:10 000) for 1 h at 4°C. Proteins were detected using the Odyssey fluorescent imager. Images were then analyzed using ImageJ software and were normalized to overall levels of the respective tubulin band. These methods were used in parallel for both Bovine and MCF7. Antibodies used: for overall tubulin levels, an Abcam murine Monoclonal antitubulin antibody, (cat no. ab56676); for poly-glutamylation, a Sigma Monoclonal murine antitubulin antibody, polyglutamylated (cat no. T9822); for tyrosination, a Sigma murine monoclonal antitubulin, tyrosine antibody (cat no. T9028), recognizing tubulin's normally present c-terminal tyrosine; for acetylation, a Sigma murine monoclonal antiacetylated tubulin antibody (cat no. T7451).

Modeling

Simulations of Eg5 motor walking on MTs were carried out using Monte Carlo approach. Load-dependent motor stepping rates and forward detachment kinetics were set as reported earlier (32,39). Briefly, we used the following theoretical relations.

Force–velocity dependence for stepping rate of motor:

$$k_{\rightarrow \text{step}}(F) = \begin{cases} \left(\frac{v}{d}\right)\left(1 - \left(\frac{F}{F_s}\right)^W\right) & F \le F_s \\ 0 & F > F_s \end{cases}$$

Exponential detachment kinetics below stall $\varepsilon(F) = \varepsilon \exp(F/F_d)$ was used for Eg5 walking on MCF7 MTs away from trap center. To simulate two different segments of velocities for Eg5 on MCF7 velocity of 100 and 24 nm/seconds were used in forward stepping rate equation.

For Eg5 on bovine MTs, the velocity is independent of load beyond certain value of applied load (~0.5pN). To simulate these tracks a constant stepping rate that is independent of load was used.

The force on the cargo due to multiple Eg5 motors working under trap, continuously changing applied load, was calculated as

$$\bar{f} = k_{\text{trap}}\left(x - x_{\text{trap}}\right) + \sum_{j=1}^{N} k_{\text{mot}} \Delta l_j$$

In the above equations, F is the force on the motor head, F_s is the stall force of the motor (5 pN), F_d is the detachment force (4.6 pN for MCF7 and 3.2pN for Bovine), v is the velocity of the motor, d is the step size of the motor (8 nm), k_{trap} is the laser trap stiffness (0.05 pN/nm), k_{mot} is the stiffness of the motor (0.32 pN/nm), Δl_j is the extension of the walking motor j beyond its rest length l (50 nm), r is the radius of the cargo (250 nm) and Δt is the the time step. In the multiple motor simulations, on-rate of motor was determined to be 0.7 seconds^{-1}. The displacements of the bead at times t and $t + \Delta t$ are related by, $x(t + \Delta t) = x(t) + x_{\text{random}} + x_{\text{drift}}$, where x_{random} is the Brownian displacement. To estimate the cargo drift, $x_{\text{drift}} = \frac{\bar{f}}{6\pi\eta r}(\Delta t)$ at the surface the viscosity η, was chosen as ~2xwater.

Acknowledgments

We thank members of the Gross laboratory for technical help and useful discussions. This work was funded by The Seton Hall University (to M.S.F), National Institutes of Health Grants GM102875-07 (to S.S.R.) and GM070676 (to S.P.G.). The authors declare no conflict of interest.

Supporting Information

Additional Supporting Information may be found in the online version of this article:

Figure S1. Characterization of Kinesin-1 moving along Bovine Brain and MCF7 microtubules. Example: force versus time traces of kinesin-1-coated beads moving along a single (A) bovine brain microtubule, or (B) MCF7 microtubule, under a moderately high-force optical trap (trap stiffness of ~0.05 pN/nm). Experiments were performed at saturating (1 mM) ATP. Histogram of typical detachment forces produced along (C) bovine brain, and (D) MCF7 microtubules are shown. The average detachment force is calculated by fitting the Gaussian distribution to the histograms, found to be 3.1 ± 0.08 pN on bovine brain microtubules (n = 141 measurements, C) and 2.8 ± 0.1 (n = 184 measurements, D) on MCF7 microtubules. Although similar, the mean value of forces in C and D are significantly different, evaluated by t-test. The distribution of binding times along the two types of microtubules is shown in E and F, and in each case was well described by a decaying exponential (red), with value of 0.4 ± 0.01 seconds (bovine) and 0.26 ± 0.05 seconds (MCF7), again statistically significantly different.

Figure S2. Post-translational modifications detected by Western blots on bovine brain and MCF7 tubulin. Bovine brain tubulin (first row) and MCF7 tubulin (second row), was probed with a pan-tubulin antibody, (A) with an acetylation-specific antibody, (B) with an Glutamylation-specific antibody, and finally (C) with a tyrosination-specific antibody recognizing native tyrosinated tubulin (as opposed to the detyrosinated modified version). (D) The amount of each modification, quantified from the above westerns, and normalized to the overall amount of tubulin detected in (A) can be found in the main text, Figure 4A.

Figure S3. Additional example traces showing EG5 moving on subtilisin-treated Bovine brain and MCF7 microtubules. Shown is a force versus time trace of a single EG5 motors moving a bead at saturating (1 mM) ATP along subtilisin-treated bovine brain (A) or MCF7 (B) MTs in an optical trap (trap stiffness ~0.05 pN/nm).

Figure S4. Characterization of kinesin-1 moving along subtilisin-treated bovine brain and MCF7 microtubules. Example force versus time traces of single-motor kinesin-1-coated beads moving along a single (A) bovine brain microtubule or (B) MCF7 microtubule, under a moderately high-force optical trap ((trap stiffness of ~0.05 pN/nm). Experiments were carried out at saturating (1 mM) ATP. Histogram of forces produced along (C) bovine brain, and D) MCF7 microtubules are

shown. The average detachment force is calculated by fitting the Gaussian distribution to the histograms, found to be 2.2 ± 0.02 pN on bovine brain microtubules ($n = 96$ measurements, C) and 2.6 ± 0.04 ($n = 91$ measurements, D).on MCF7 microtubules. The distribution of binding times along the two types of microtubules is shown in (E) and (F), and in each case was well described by a decaying exponential (red), with value of 0.2 ± 0.01 seconds (bovine) and 0.28 ± 0.02 seconds (MCF7).

Figure S5. Characterization of single and multiple Eg-5 motors moving along bovine brain microtubules. Example: force-versus-time traces of beads incubated with low (A, single-motor) or high (B) Eg5 concentrations, moving along bovine brain microtubule in an optical trap (trap stiffness of ~0.05 pN/nm). Experiments were performed at saturating (1 mM) ATP. Histogram of corresponding forces (C) and times (D) for single-motor beads, as well as for the higher concentration beads (E, F). The average detachment forces (2.5 ± 0.05 pN, $n = 119$ measurements, C and 2.2 ± 0.11, n = 60, (D) were calculated by fitting the Gaussian distribution to the histograms. Distribution binding times were well described by a decaying exponentials (red), with value of 0.6 ± 0.01 seconds (single, E) and 0.62 ± 0.01 seconds (multiple, F).

References

1. Block SM, Goldstein LS, Schnapp BJ. Bead movement by single kinesin molecules studied with optical tweezers. Nature 1990;348:348–352.
2. Vale RD. The molecular motor toolbox for intracellular transport. Cell 2003;112:467–480.
3. Svoboda K, Schmidt CF, Schnapp BJ, Block SM. Direct observation of kinesin stepping by optical trapping interferometry. Nature 1993;365:721–727.
4. Vale RD, Funatsu T, Pierce DW, Romberg L. Direct observation of single kinesin molecules moving along microtubules. Nature 1996;380:451–453.
5. Valentine MT, Fordyce PM, Krzysiak TC, Gilbert SP, Block SM. Individual dimers of the mitotic kinesin motor eg5 step processively and support substantial loads in vitro. Nat Cell Biol 2006;8:470–476.
6. Crevel IM, Lockhart A, Cross RA. Kinetic evidence for low chemical processivity in ncd and Eg5. J Mol Biol 1997;273:160–170.
7. Rosenfeld SS, Xing J, Jefferson GM, King PH. Docking and rolling–a model of how the mitotic motor Eg5 works. J Biol Chem 2005;280:35684–35695.
8. Svoboda K, Block SM. Force and velocity measured for single kinesin molecules. Cell 1994;77:773–784.
9. Mattson-Hoss MK, Niitani Y, Gordon EA, Jun Y, Bardwell L, Tomishige M, Gross SP. CK2 activates kinesin via induction of a conformational change. Proc Natl Acad Sci USA 2014;111:7000–7005.
10. Visscher K, Schnitzer MJ, Block SM. Single kinesin molecules studied with a molecular force clamp. Nature 1999;400:184–189.
11. Goulet A, Major J, Jun Y, Gross SP, Rosenfeld SS, Moores CA. A comprehensive structural model of the mechanochemical cycle of a mitotic motor highlights molecular adaptations in the kinesin family. Proc Natl Acad Sci USA 2014;111:1837–1842.
12. Kaan HY, Major J, Tkocz K, Kozielski F, Rosenfeld SS. "Snapshots" of ispinesib-induced conformational changes in the mitotic kinesin Eg5. J Biol Chem 2013;288:18588–18598.
13. Goulet A, Behnke-Parks WM, Sindelar CV, Major J, Rosenfeld SS, Moores CA. The structural basis of force generation by the mitotic motor kinesin-5. J Biol Chem 2012;287:44654–44666.
14. Turner J, Anderson R, Guo J, Beraud C, Fletterick R, Sakowicz R. Crystal structure of the mitotic kinesin Eg5 reveals a novel conformation of the neck-linker. J Biol Chem 2001;276:25496–25502.
15. Ogawa T, Nitta R, Okada Y, Hirokawa N. A common mechanism for microtubule destablilizer–M type kinesins stabilize curling of the protofilament using the class-specific neck and loops. Cell 2004;116:591–602.
16. Zhang D, Asenjo AB, Grrebaum M, Xie L, Sharp DJ, Sosa H. A second tubulin binding site on the kinesin-13 motor head domain is important during mitosis. PLoS One 2013;8:e73075.
17. Soppina V, Verhey KJ. The family-specific K-loop influences the microtubule on-rate but not the superprocessivity of kinesin-3 motors. Mol Biol Cell 2014;25:2161–2170.
18. Waitzman JS, Larson AG, Cochran JC, Naber N, Cooke R, Jon Kull F, Pate E, Rice SE. The loop 5 element structurally and kinetically coordinates dimers of the human kinesin-5, Eg5. Biophys J 2011;101:2760–2769.
19. Walter WJ, Beranek V, Fischermeier E, Diez S. Tubulin acetylation alone does not affect kinesin-1 velocity and run length in vitro. PLoS One 2012;7:e42218.
20. Kaul N, Soppina V, Verhey KJ. Effects of a-tubulin K40 acetylation and detyrosination on kinesin-1 motility in a purified system. Biophys J 2014;106:2636–2643.
21. Herms A, Bosch M, Reddy B, Schieber NL, Fajardo A, Ruperez C, Fernandez-Vidal A, Ferguson C, Rentero C, Tebar F, Enrich C, Patron RG, Gross SP, Pol A. AMPK activation promotes lipid droplet dispersion on detyrosinated microtubules to increase mitochondrial fatty acid oxidation. Nat Commun 2015;27:7176–7190.
22. Konishi Y, Setou M. Tubulin tyrosination navigated the kinesin-1 motor domain to axons. Nat Neurosci 2009;12:559–567.
23. Barisic M, Silvia e Sousa R, Tripathy SK, Magiera MM, Zaytsev AV, Pereira AL, Janke C, Grishchuk EL, Maiato H. Mitosis: microtubule detyrosination guides chromosomes during mitosis. Science 2015;348:799–803.
24. Peris L, Wagenbach M, Lafanechere L, Brocard J, Moore AT, Kozielski F, Job D, Wordeman L, Andrieux A. Motor-dependent microtubule disassembly driven by tubulin tyrosination. J Cell Biol 2009;185:1159–1166.
25. Dunn S, Morrison EE, Liverpool TB, Molina-Paris C, Cross RA, Alonso MC, Peckham M. Differential trafficking of Kif5c on tyrosinated and detyrosinated microtubules in live cells. J Cell Sci 2008;121:1085–1095.
26. Sirajuddin M, Rice LM, Vale RD. Regulation of microtubule motors by tubulin isotypes and post-translational modifications. Nat Cell Biol 2014;16:335–344.
27. Mallik R, Gross SP. Intracellular transport: how do motors work together. Curr Biol 2009;19:R416–R418.
28. 28 Shubeita G, Tran S, Xu J, Vershinin M, Cermelli S, Cotton S, Welte M, Gross SP. Consequences of motor copy number on the intracellular

transport of kinesin-1-driven lipid droplets. Cell 2008;135:1098–1107.
29. Hendricks AG, Holzbaur EL, Goldman YE. Force measurements on cargoes in living cells reveal collective dynamics of microtubule motors. Proc Natl Acad Sci USA 2012;109:18447–18452.
30. Leidel C, Longoria RA, Gutierrez FM, Shubeita G. Measuring molecular motor forces in vivo: implications for Tug of War models of bidirectional transport. Biophys J 2012;103:492–500.
31. Rai AK, Rai A, Ramaiya AJ, Jha R, Mallik R. Molecular adaptations allow dynein to generate large collective forces inside cells. Cell 2013;152:172–182.
32. Kunwar A, Tripathy SK, Xu J, Mattson MK, Anand P, Sigua R, Vershinin M, McKenney RJ, Yu CC, Mogilner A, Gross SP. Mechanical stochastic tug-of-war models cannot explain bidirectional lipid-droplet transport. Proc Natl Acad Sci USA 2011;108:18960–18965.
33. McKenney RJ, Vershinin M, Kunwar A, Vallee RB, Gross SP. LIS1 and NudE induce a persistent dynein force-producing state. Cell 2010;141:304–314.
34. Xu J, Shu Z, King SJ, Gross SP. Tuning multiple motor travel via single motor velocity. Traffic 2012;13:1198–1205.
35. Feizabadi MS, Jun Y. Kinesin-1 translocation: surprising differences between bovine brain and MCF7-derived microtubules. Biochem Biophys Res Commun 2014;454:543–546.
36. Duselder A, Thiede C, Schmidt CF, Lakamper S. Neck-linker length dependence of processive kinesin-5 motility. J Mol Biol 2012;423:159–168.
37. Lakamper S, Thiede C, Duselder A, Reiter S, Korneer MJ, Kapitein LC, Peterman EJG, Schmidt CF. The effect of monastrol on the processive motility of dimeric kinesin-5 head/kinesin-1 stalk chimera. J Mol Biol 2010;339:1–8.
38. Shastry S, Hancock WO. Interhead tension determines processivity across diverse N-terminal kinesins. Proc Natl Acad Sci USA 2011;108:16253–16258.
39. Kunwar A, Vershinin M, Xu J, Gross SP. Stepping, strain gating, and an unexpected force velocity curve for multiple-motor-based transport. Curr Biol 2008;18:1173–1183.
40. Vershinin M, Carter BC, Razafsky DS, King SJ, Gross SP. Multiple-motor based transport and its regulation by Tau. Proc Natl Acad Sci USA 2007;104:87–92.
41. Banerjee A, Luduena RF. Kinetics of colchicine binding to purified b-tubulin isotypes from bovine brain. J Biol Chem 1992;267:13335–13339.
42. Davis A, Martinez S, Nelson D, Middleton K. A tubulin polymerization microassay used to compare ligand efficacy. Methods Cell Biol 2010;95:327–347.
43. Wang Z, Sheetz MP. The C-terminus of tubulin increases cytoplasmic dynein and kinesin processivity. Biophys J 2000;78:1955–1964.
44. Jamison DK, Driver JW, Rogers AR, Constantinou PE, Diehl MR. Two kinesins transport cargo primarily via the action of one motor: implications for intracellular transport. Biophys J 2010;99:2967–2977.
45. Driver JW, Jamison DK, Uppulury K, Rogers AR, Kolomeisky AB, Diehl MR. Productive cooperation among processive motors depends inversely on their mechanochemical efficiency. Biophys J 2011;101:386–395.
46. Klumpp S, Lipowsky R. Cooperative cargo transport by several molecular motors. Proc Natl Acad Sci USA 2005;102:17284–17289.
47. Mallik R, Carter BC, Lex SA, King SJ, Gross SP. Cytoplasmic dynein functions as a gear in response to load. Nature 2004;427:649–652.
48. Mallik R, Petrov D, Lex SA, King SJ, Gross SP. Building complexity: an in vitro study of cytoplasmic dynein with in vivo implications. Curr Biol 2005;15:2075–2085.
49. Jun Y, Tripathy SK, Narayanareddy BRJ, Mattson-Hoss MK, Gross SP. Calibration of optical tweezers for in vivo force measurements: how do different approaches compare?" Biophys J 2014;107:1474–1484.